Petroleum Science 20 (2023) 3540–3552

Contents lists available at ScienceDirect

Petroleum Science

journal homepage: www.keaipublishing.com/en/journals/petroleum-science

Original Paper

Intermolecular interactions induced property improvement for clean fracturing fluid by deep eutectic solvents

Xiang-Yu Wang [a, b], Ming-Wei Zhao [a, b, **], Xu-Hao Wang [c], Peng Liu [a, b], Meng-Yao Fan [a, b], Teng Li [a, b], Zhen-Feng Ma [a, b], Ying-Jie Dai [a, b], Cai-Li Dai [a, b, *]

[a] Key Laboratory of Unconventional Oil & Gas Development, China University of Petroleum, Qingdao, 266580, Shandong, PR China
[b] Shandong Key Laboratory of Oilfield Chemistry, China University of Petroleum, Qingdao, 266580, Shandong, PR China
[c] Dongxin Oil Production Plant Ying First Management Zone of Sinopec Shengli Oilfield Company, Dongying, 257002, Shandong, PR China

ARTICLE INFO

Article history:
Received 18 December 2022
Received in revised form
8 August 2023
Accepted 9 August 2023
Available online 11 August 2023

Edited by Yan-Hua Sun

Keywords:
Deep eutectic solvents (DESs)
Clean fracturing fluids (CFFs)
Intermolecular interactions
Property improvement

ABSTRACT

Fracturing fluid property play a critical role in developing unconventional reservoirs. Deep eutectic solvents (DESs) show fascinating potential for property improvement of clean fracturing fluids (CFFs) due to their low-price, low-toxicity, chemical stability and flexible designability. In this work, DESs were synthesized by mixing hydrogen bond acceptors (HBAs) and a given hydrogen bond donor (HBD) to explore their underlying influence on CFF properties based on the intermolecular interactions. The hydrogen-bonding, van der Waals and electrostatic interactions between DES components and surfactants improved the CFF properties by promoting the arrangement of surfactants at interface and enhancing the micelle network strength. The HBD enhanced the resistance of CFF for Ca^{2+} due to coordination-bonding interaction. The DESs composed of choline chloride (ChCl) and malonic acid show great enhancement for surface, rheology, temperature resistance, salt tolerance, drag reduction, and gel-breaking performance of CFFs. The DESs also improved the gel-breaking CFF-oil interactions, increasing the imbibition efficiencies to 44.2% in 74 h. Adjusting HBAs can effectively strengthen the intermolecular interactions (e.g., HBA-surfactant and HBD-surfactant interactions) to improve CFF properties. The DESs developed in this study provide a novel strategy to intensify CFF properties.

1. Introduction

In the past decade years, the development of unconventional reservoirs containing abundant oil has aroused growing concerns to cope with the depleting conventional reservoirs and increasing energy demands (Wang et al., 2022; Zhang et al., 2022a). However, the low permeability and low porosity of unconventional reservoirs result in huge difficulty of development and low oil recovery (Lee et al., 2016; Yin et al., 2022). Water-based fracturing fluid is an important means to effectively enhance oil recovery (Yang et al., 2022). Macromolecule polymers (e.g., synthesized polymer (Zhang et al., 2018) and guar gum (Wu et al., 2023)), as thickeners of traditional water-based fracturing fluids, can generate plenty of residues after gel breaking, damaging reservoirs (Ma et al., 2022; Zhao et al., 2019).

Clean fracturing fluids (CFFs) prepared by viscoelastic surfactants can sharply reduce the reservoir damage due to no residues after gel breaking (Zhao et al., 2019). Viscoelastic surfactants can spontaneously self-assemble into micelles to impart viscoelasticity to CFFs (Scholz et al., 2021). The gel breaking of CFFs can be completed by simply contacting with oil in the reservoirs, no additional gel breakers are required, thus, reducing formation damage and environmental pollution (Chu et al., 2013). After gel breaking, surfactants in CFFs can decrease oil–water interfacial tension (IFT) and change reservoir wettability to improve spontaneous imbibition efficiency (de Aguiar et al., 2010; Javadi and Fatemi, 2022; Zhang et al., 2021b). Li and co-workers (Li et al., 2022) reported that the CFF with 0.7% oleamidopropyl dimethylamine and 0.7% sodium *p*-toluenesulfonate removed 27.0% of oil

* Corresponding author. Key Laboratory of Unconventional Oil & Gas Development, China University of Petroleum, Qingdao, 266580, Shandong, PR China.
** Corresponding author. Key Laboratory of Unconventional Oil & Gas Development, China University of Petroleum, Qingdao, 266580, Shandong, PR China.
E-mail addresses: zhaomingwei@upc.edu.cn (M.-W. Zhao), daicl@upc.edu.cn (C.-L. Dai).

https://doi.org/10.1016/j.petsci.2023.08.013

from low-permeability cores for 150 h. Liu et al. (2019) found that the imbibition efficiency of oil could reach up to 34.6% in 0.1 wt% sodium alcohol ether sulphate surfactant solution. In order to obtain higher oil recovery, nanoparticles have been employed as enhancers to further improve spontaneous imbibition performance of fracturing fluids by reducing oil–liquid IFT and changing wettability of rock surface (Kuang et al., 2018; Zhou et al., 2019c). Nanoparticles can also improve rheological properties of clean fracturing fluids due to the formation of non-covalent bonds with micelles (Raj et al., 2022). However, the application of nanoparticles faces the dilemma in poor stability caused by environmental changes such as temperature, salinity and pH (Cheng et al., 2013; Zhang et al., 2020). Besides, agglomerated nanoparticles even result in reservoir blocking during the oil development process (Liu et al., 2020). To solve these issues, novel functional enhancers are urgent to be developed.

The potential of ionic liquids (ILs) for enhanced oil recovery have been confirmed (Sakthivel et al., 2016). However, high price, toxicity and poor biodegradability restrict their large-scale use (Zhang et al., 2012). Deep eutectic solvents (DESs), as a promising alternative of ILs, have many advantages such as low-price, non-toxicity, biodegradability, chemical stability, non-volatility, flexible designability (Jin et al., 2022; Tran et al., 2019). DESs can be simply synthetized by only mixing hydrogen bond acceptors (HBAs such as ammonium salt) and hydrogen bond donors (HBDs such as acids, amines and alcohols) without by-products, which is considered a green preparation method (Wang et al., 2021). To date, DESs have been applied in many fields (e.g., catalysis (Zhou et al., 2019b), material preparation (Smith et al., 2014), electrochemistry (Wang et al., 2021), purification process (Xie et al., 2016) etc.). Nowadays, more and more works have focus on the application of DES to petroleum development. With the addition of choline chloride-glycerol DES, Hadj-Kali and co-workers (Hadj-Kali et al., 2015) reported that the oil/brine IFT was decreased from 24.11 to 0.072 $mN \cdot m^{-1}$. Sanati et al. (2021) found that the choline chloride-citric acid DES solution reduced crude oil/brine IFT from 31.0 to 6.1 $mN \cdot m^{-1}$ and altered the wettability of rock surface from oil-wet to water-wet. Atilhan and Aparicio (2022) used molecular dynamics simulations to study the ability of choline chloride-based DESs to decrease the oil-water IFT and change the rock-surface wettability. These studies suggest that DESs have presented a considerable potential for strengthening the imbibition performance of clean fracturing fluids. What's more, it seems that HBD components in DESs are able to enhance the strength of micelle networks of CFFs by forming intermolecular interactions owing to the functional groups (e.g., −OH, $-SO_3H$, and −COOH) of HBDs and viscoelastic surfactants (Li et al., 2018b). Driven by the intrinsic hydrogen-bonding interactions in DESs, the HBA components with almost no functional group may also affect CFF properties (Zhang et al., 2012). To the best of our knowledge, no work has paid attention to the possible effects on enhancing the CFF properties.

In this case, a novel method for enhancing fracturing fluid properties using DESs is firstly reported. Four DESs were synthetized by heating the mixture of malonic acid (a given HBD) and HBAs (ammonium compounds). Then, five octadecylamide hydroxypropyl sulfonbetaine (OAHSB)-based CFFs with or without DESs were prepared, and their properties (e.g., rheology, drag reduction and spontaneous imbibition performances) were measured to investigate the impact of DESs. Moreover, it is revealed that selecting suitable HBAs plays an important role in improving the properties of fracturing fluids. The DESs supplied a novel route to effective enhancement of CFF properties.

2. Experimental

2.1. Chemicals

Choline chloride (ChCl, ≥ 98.0% purity), tetraethylammonium chloride (TEAC, ≥ 98.0% purity), tetrabutylammonium chloride (TBAC, ≥ 97.0% purity), tetramethylammonium chloride (TMAC, ≥ 98.0% purity), malonic acid (≥ 99.0% purity), stearic acid (≥ 98.0% purity), sodium hydroxide (≥ 98.0% purity), potassium hydroxide (≥ 95.0% purity), 3-(dimethylamino)-1-propylamine (DMAPA, ≥ 99.0% purity), sodium 3-chloro-2-hydroxypropanesulfonate (CHPS, ≥ 95.0% purity), ethanol (≥ 99.5% purity), isopropyl alcohol (≥ 99.7% purity), sodium chloride (≥ 99.5% purity), calcium chloride (≥ 96.0% purity), dodecyl mercaptan (≥ 99.5% purity), petroleum ether, bromophenol blue and phenolphthalein indicators were purchased from Aladdin Industrial Inc., China. Crude oil and cores samples were obtained from Changqing Oilfields. Kerosene was achieved from Sinopec Qingdao Refining & Chemical Co., Ltd. Ultrapure water (18.2 MΩ·cm at 25 °C) was prepared by a water processor.

2.2. Preparation of DESs and simulated oil

The DESs were synthesized by mixing HBA and HBD at a molar ratio of 1:2 in a round bottom flask, followed by vigorous stirring at 80–100 °C for 3 h. After HBA and HBD compositions were transformed into a homogeneous liquid phase, the as-prepared DESs were dried under high vacuum at 60 °C for 24 h, and then placed in a desiccator for further utilization. Fig. 1 exhibits the structures of HBD and HBAs used in this work. The compositions of DESs are shown in Table 1.

The simulated oil was prepared under mechanical stirring to fully mix crude oil and kerosene with a molar ratio of 1:10. The density of simulated oil was 0.81 $g \cdot cm^{-3}$.

2.3. Synthesis of OAHSB

The OAHSB was synthesized as the following two steps (see Supporting information, Fig. S1) (Feng et al., 2012; Kelleppan et al., 2021):

(1) Stearic acid was completely melted by heating in a three-necked flask with a mechanical stirrer at 90 °C. DMAPA and NaOH were mixed with stearic acid in turn at the NaOH/stearic acid mass ratio of 0.006:1 and stearic acid/DMAPA molar ratio of 1:1.2. The mixture was then reacted at 140 °C

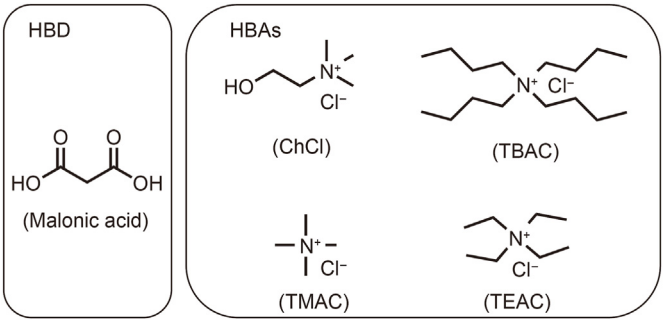

Fig. 1. Structures of HBD and HBAs used in formation of DESs.

Table 1
Compositions of DESs utilized in this study.

Abbreviation	HBAs	HBD	Molar ratio of HBA to HBD
D1	ChCl	Malonic acid	1:2
D2	TMAC	Malonic acid	1:2
D3	TEAC	Malonic acid	1:2
D4	TBAC	Malonic acid	1:2

for 10 h. The product was purified in vacuo and recrystallization via petroleum ether, and stearamidopropyl dimethylamine (SAPDA) was obtained. The effect of reaction parameters, including the mass ratio of NaOH/stearic, molar ratio of stearic acid/DMAPA, reaction time, and reaction temperature, are shown in Figs. S2–S5 (Supporting information).

(2) The water and ethanol were chosen as the solvent to dissolve the CHPS and prepared SAPDA, respectively, followed by mixing and heating at 90 °C for 8 h. The solvent of crude product was removed using vacuum rotary evaporation. The as-synthesized OAHSB was washed and recrystallized by petroleum ether and isopropyl alcohol, and then dried in a freezing dryer. Detailed operation conditions are presented in Figs. S6–S9 (Supporting information). The product was analyzed through Fourier transform infrared (FT-IR) spectrometer and hydrogen nuclear magnetism (^{1}H-NMR) spectrogram (see Supporting information, Figs. S10 and S11).

2.4. Preparation of CFFs and gel-breaking CFFs

The OAHSB-based CFFs were obtained by adding OAHSB, TsONa and DESs to water at a mass ratio (OAHSB:TsONa:DES) of 1:0.5:1.5 (or 1:0.5:0), followed by stirring to form homogeneous liquid phase. The compositions of CFFs are listed in Table 2. CFFs were mixed with kerosene by stirring at room temperature until the gel broke. Then, the mixtures were settled for another 30 min to ensure thorough separation of kerosene (upper phase) and gel-breaking CFFs (bottom phase). The gel-breaking CFFs phases were collected into sample bottles for subsequent use.

2.5. Drag reduction measurement

A fracturing fluid friction tester (see Figs. S12) was applied to determine the drag reduction efficiencies of CFFs. The tester was firstly calibrated with water. Then, the CFF solution was pumped into the tester. The experimental parameters (i.e., temperature and liquid flow rate) were programmed by software. After the tester reached the set temperature, the CFF solution was circulated in closed pipeline at a given flow rate for 10 min to obtain stable pressure drop. The drag reduction efficiency (D_R) was calculated from the following equation:

$$D_R = \frac{\Delta P_0 - \Delta P_1}{\Delta P_0} \quad (1)$$

where ΔP_0 and ΔP_1 represent the pressure drops formed by water and CFFs in the tester tubing, respectively.

2.6. Gel-breaking measurement

The CFF was mixed with kerosene at a certain CFF:kerosene mass ratio at 25 °C for 5 min. After mixture, another 10 min was needed to separate the CFF phase (bottom layer) from the kerosene phase (upper layer). The viscosity of the CFF phase was measured using a rheometer.

2.7. Spontaneous imbibition measurement

Core samples were vacuum saturated with simulated oil for 24 h, and aged in an oven at 80 °C for 14 days. The saturated core was placed into the sealed imbibition bottle with gel-breaking CFF at 80 °C. During imbibition process, the volume of imbibed oil at different times was recorded. The imbibition efficiency (I_e) of CFFs was calculated as follows:

$$I_e = \frac{c \cdot V_t}{W_2 - W_1} \quad (2)$$

where c denotes the density of oil; V_t represents the volume of imbibed oil; W_2 and W_1 are the primary and saturated core mass, respectively.

2.8. Analytical methods

The rheological behavior of CFFs were analyzed by the rheometer (Haake Mars 60) with CC41/Ti barrel rotor. Tracker automatic tensiometer was used to obtain the surface tension of solutions. The oil–water IFT was measured by the spinning drop interfacial tensiometer (TX 500 C, Kono, USA). A laser particle size analyzer (Zetasizer Nano ZS90, England) was utilized to measure the dynamic light scattering (DLS) and zeta potential of CFFs. The surface tension was measured using the Tracker automatic tensiometer. A FT-IR (Bruker, Germany) spectrometer was employed to characterized compounds. ^{1}H-NMR spectra was recorded on the Bruker 400 MHz spectrometer. The heteroatom content in simulated oil was obtained through the elemental analyzer (Vario EL III, German).

A Bruker atomic force microscope (AFM) was used to analyze the adhesion in gel-breaking CFFs between probe and hydrophilic glass sheet under AFM force volume mode at room temperature. The probe was immersed in ethanol solution with a dodecyl mercaptan concentration of 10 mmol·L^{-1} for 24 h, followed by washing with ethanol and drying with N_2 to obtain hydrophobicity.

3. Results and discussion

3.1. Surface properties

The surface tension (γ) of OAHSB-based CFF systems is shown in Fig. 2(a). It can be seen that γ sharply decreases with the increase in

Table 2
Compositions of CFFs applied in this study.

Abbreviation	Surfactant	Salt	DESs	Molar ratio of surfactant to salt to DES
F0	OAHSB	TsONa	–	1:0.5
F0-D1	OAHSB	TsONa	D1	1:0.5:1.5
F0-D2	OAHSB	TsONa	D2	1:0.5:1.5
F0-D3	OAHSB	TsONa	D3	1:0.5:1.5
F0-D4	OAHSB	TsONa	D4	1:0.5:1.5

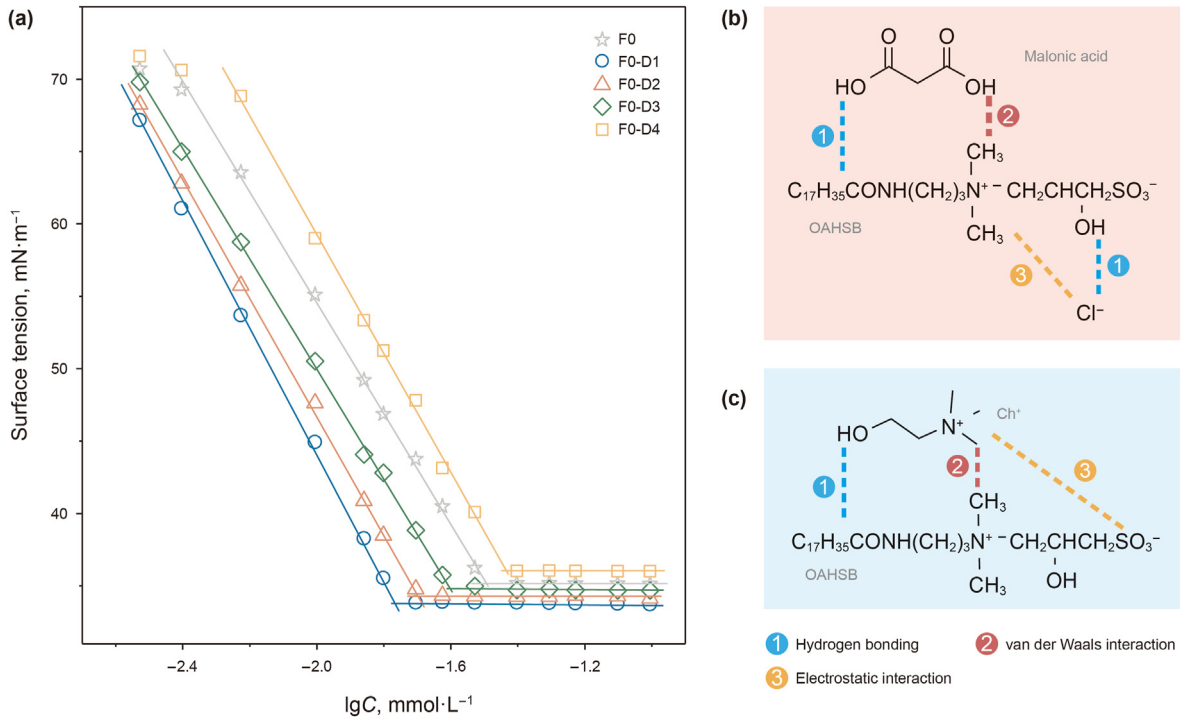

Fig. 2. (**a**) Plot of surface tension versus surfactant concentration for F0, F0-D1, F0-D2, F0-D3 and F0-D4 systems. Schematic hydrogen-bonding interactions, van der Waals interactions and electrostatic interactions between malonic acid/Cl^- and OAHSB (**b**), and between Ch^+ and OAHSB (**c**).

surfactant concentration (C) below the critical micelle concentration (CMC). After the surfactant concentration achieved CMC, γ is weakly changed. The different CMC values for the CFFs demonstrate that the D1-D4 DESs affect the formation of micelles. For example, micelle formation is promoted by D1 and inhibited by D4. Although γ value is closely related to the adsorption of surfactant molecules at air/water surface, different γ values for those solutions imply that DESs affect the adsorption of OAHSB. D1-D3 components facilitate the compact arrangement of OAHSB molecules at interface and thus reduce the γ_{cmc} of F0 from 35.1 to 33.8–34.7 $mN \cdot m^{-1}$. After introducing D4, the γ_{cmc} of F0 is found to slightly increase to 36.0 $mN \cdot m^{-1}$.

To further explore the adsorption of OAHSB in the CFFs at interface, the maximum adsorption amount of surfactant (Γ_{max}) was subsequently analyzed by Gibbs adsorption equation (Eq. (3)) (Rosen, 2004):

$$\Gamma_{max} = -\frac{1}{2.303nRT}\left(\frac{\partial r}{\partial \lg C}\right) \quad (3)$$

where R denotes thermodynamic constant, $J \cdot mol^{-1} \cdot K^{-1}$; T means Kelvin temperature, K. Because the electrolyte concentration of the CFF systems is much higher than CMC, n is defined as 1 (Zhang et al., 2022b).

The Γ_{max} values of surfactants in CFFs increase in the order of F0-D4 (1.60×10^{-6} $mol \cdot m^{-2}$) < F0 (1.97×10^{-6} $mol \cdot m^{-2}$) < F0-D3 (2.81×10^{-6} $mol \cdot m^{-2}$) < F0-D2 (3.46×10^{-6} $mol \cdot m^{-2}$) < F0-D1 (3.78×10^{-6} $mol \cdot m^{-2}$) as shown in Table 3. It seems that the HBAs with small molecule size in DESs could lead to an intense arrangement of OAHSB at interface. According to the Γ_{max} values, the minimum area of per OAHSB molecule (A_{min}) can be calculated from (Rosen, 2004):

$$A_{min} = \frac{1}{N_A \Gamma_{max}} \quad (4)$$

where N_A represents Avogadro constant.

A low A_{min} means a denser arrangement of OAHSB molecule at the air–solution interface. For F0-D1, F0-D2 and F0-D3, the relatively low A_{min} further confirms that the D1–D3 can help tightening the arrangement of OAHSB (see Table 3). It is probably attributed to the malonic acid-OAHSB and OAHSB-Cl^- hydrogen-bonding interactions, van der Waals interaction and electrostatic interactions (see Fig. 2(b)). In addition to the OAHSB-Ch^+ van der Waals interaction and electrostatic interactions (Kawai et al., 2016), the OAHSB-Ch^+ hydrogen-bonding interaction should be the reason for the minimum A_{min} value of F0-D1 (see Fig. 2(c)). Moreover, the largest A_{min} of F0-D4 illustrates that the large steric hindrance of TBAC can restrain the formation of strong interactions (e.g., malonic acid-OAHSB interaction), relaxing the arrangement of OAHSB (Su et al., 2007).

Table 3
Parameters of surface activity for OAHSB-based solutions.

CFFs	CMC, mM	γ_{CMC}, $mN \cdot m^{-1}$	$10^{-6}\Gamma_{max}$, $mol \cdot m^{-2}$	A_{min}, nm^2
F0	0.032	35.1	1.97	0.84
F0-D1	0.017	33.8	3.78	0.44
F0-D2	0.020	34.1	3.46	0.48
F0-D3	0.025	34.7	2.81	0.59
F0-D4	0.037	36.0	1.60	1.04

3.2. Rheological properties of CFFs

The influence of DESs on viscosity of F0 at 170 s^{-1} was explored using F0 with or without D1–D4 (see Fig. 3(a)). After the addition of D1–D3, the viscosity of F0 system was increased from 39.2 to 47.3–58.4 mPa·s. It is probably ascribed to the interactions (e.g., O···H–O hydrogen bond) between DES components and OAHSB, enhancing the entanglement of micelles in F0. Differently, D4 decreases the viscosity of F0 from 39.2 to 24.4 mPa·s. The decreased

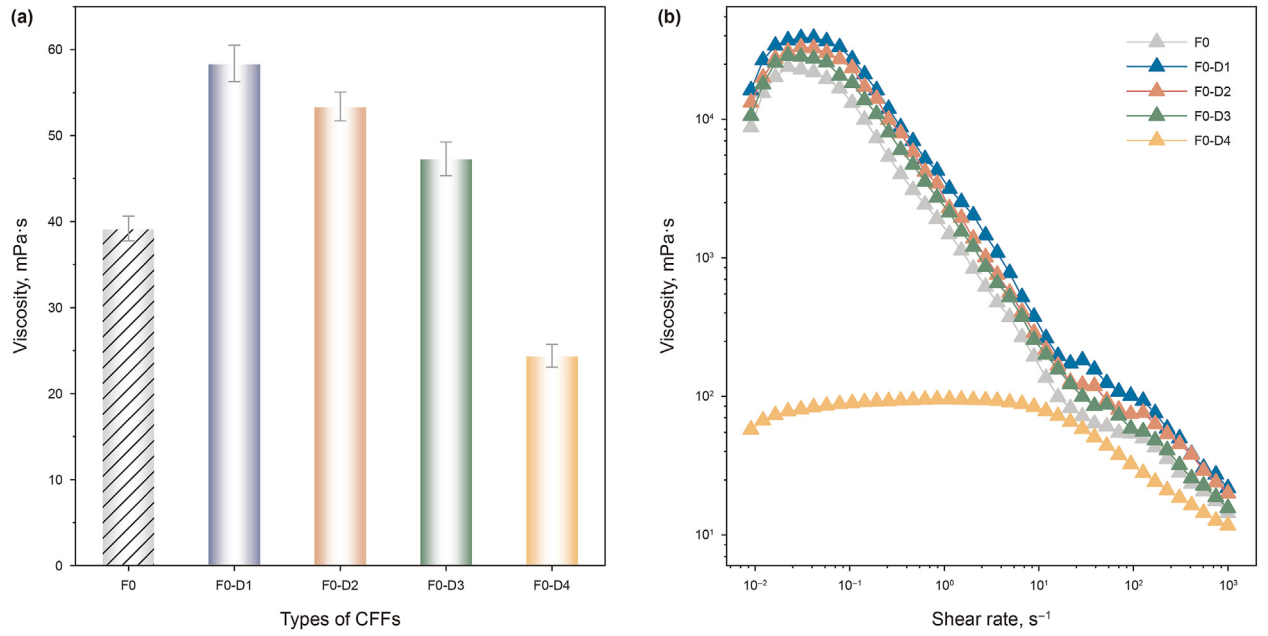

Fig. 3. (**a**) Viscosity at 170 s^{-1} and (**b**) steady shear viscosity of OAHSB-based CFFs.

viscosity may be ascribed to the large steric hindrance of TBAC in D4, hindering the formation of micelles. These results indicate that DESs can also influence the viscosity of CFF. Adjusting the HBA components of DESs further alter the viscosity.

The steady shear performance of CFFs is shown in Fig. 3(b). The viscosities of those CFFs are initially improved at low shear rates, mainly induced by tight entangling of micelles under shear force. As the increase in shear rate, the shear thinning behavior of CFFs can be observed because the micelle networks are gradually destroyed under stronger shear force, matching the typical feature of non-Newtonian fluid (Hao et al., 2020). F0-D4 shows a unique feature consistent with Newtonian fluid at shear rate of 0.02–6.67 s^{-1}. Namely, the viscosity is hardly changed upon changing shear rate. Compared with F0 system, F0-D1, F0-D2 and F0-D3 have larger zero-shear viscosities and their viscosity peaks occur at higher shear rates, suggesting the enhancement of D1–D3 for shear resistance of CFFs due to increased micelle network strength (Zhang et al., 2020). The increase in micelle network strength may be mainly due to the HBD (i.e., malonic acid) in D1–D3, which acts as a crosslinker in the CFF system to increases the entanglement of the micelle network. The lowest zero-shear viscosity (94.8 mPa·s) of F0-D4 implies the negative effect of D4 on micelle network strength. Clearly, in the F0-D4 system, the effect of TBAC HBA in D4 on the micelle network strength exceeds that of malonic acid.

The oscillatory rheological date (storage moduli (G') and loss moduli (G'')) for the five OAHSB-based CFFs as depicted in Fig. 4. F0, F0-D1, F0-D2 and F0-D3 mainly show viscoelastic characteristics ($G' > G''$) at low oscillatory frequency and viscous characteristics ($G'' > G'$) at high oscillatory frequency. In contrast, F0-D4 CFF presents opposite characteristics, demonstrating TBAC of D4 alters the oscillatory rheological behavior of F0. The intersection points of G' and G'' indicate that all five OAHSB-based CFFs have viscoelasticity because of the formation of wormlike micelle network (Zhang et al., 2022b). According to the critical angular frequency (ω_c) and critical moduli value (G_c) corresponding to the intersection point, the plateau moduli (G_0) and relaxation time (τ_R) can be calculated from Eqs. (5) and (6) (Acharya et al., 2006):

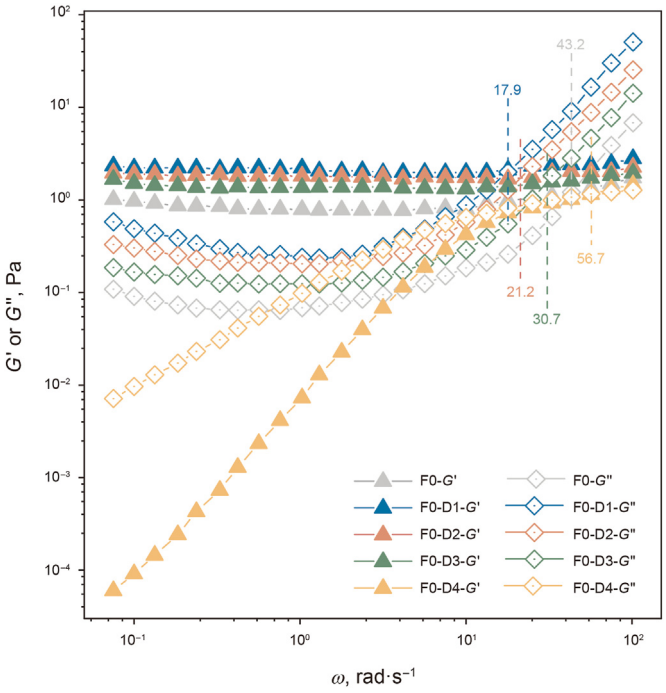

Fig. 4. Oscillatory rheological behavior of OAHSB-based CFFs as a function of frequency (ω).

$$G_0 = 2G_c \tag{5}$$

$$\tau_R = \frac{1}{\omega_c} \tag{6}$$

The larger the G_0 and τ_R values, the closer the entanglement of micelle network. From Table 4, the G_0 of F0-D1, F0-D2, F0-D3 are 2.94, 3.42 and 4.06 Pa, respectively, which are higher than that of F0 (2.44 Pa), demonstrating that the D1-D3 DESs enhance the

Table 4
Rheological parameters for the OAHSB-based CFFs.

CFFs	G_c, Pa	G_0, Pa	ω_c, rad·s^{-1}	τ_R, s
F0	1.22	2.44	43.2	0.023
F0-D1	2.03	4.06	17.9	0.056
F0-D2	1.71	3.42	21.2	0.047
F0-D3	1.47	2.94	30.7	0.032
F0-D4	1.16	2.32	56.7	0.017

entanglement density of micelle network. Conversely, the G_0 of F0-D4 is only 2.32 Pa, owing to the limit of D4 for the entanglement of micelle. The τ_R values also reflect that the entanglement density of F0 is promoted/inhibited by D1–D3/D4. The highest G' and G'' for F0-D1 can be explained by close micelle entanglement. These results suggest that only adjustments to the HBAs of DESs are needed to regulate the rheology property of CFFs.

According to the mentioned above, it can be deduced that the DESs may affect the rheological characteristics of CFFs by affecting the formation of micelles. In order to further prove the influence of DESs, efforts were devoted to analyze the component affinity and micelle size of CFFs through zeta potential and DLS results. According to the zeta potential data (Fig. 5(a)), F0 has a low zeta potential of −24.4 mV, whereas F0-D1, F0-D2 and F0-D3 exhibit larger negative zeta potential (from −26.7 to −32.1 mV), suggesting that D1–D3 give rise to the higher binding affinity of CFF components (Wu et al., 2019). For F0-D4, the reduced zeta potential contributes to a negative effect of D4 on the binding affinity of F0. DLS results show the improvement by D1–D3 and the reduction by D4 for the micelle size of F0 (Fig. 5(b)). This demonstrates that DESs can regulate the binding affinity of CFF components and thus impact the self-assembly and entanglement of micelles.

The interactions between the DES components and OAHSB molecules are considered to be a prominent factor for changing the affinity of CFF components. A typical peak appeared at 3447 cm^{-1} belongs to the O–H peak of OAHSB as indicated by FT-IR spectrum (see Fig. 5(c)). In the presence of malonic acid, the O–H peak moved to 3419 cm^{-1}, exhibiting the formation of hydrogen-bonding interactions between malonic acid and OAHSB. Similarly, the O–H peak of OAHSB shows a decreased chemical shift upon mixing OAHSB with ChCl. And the O–H peak of ChCl at 3252 cm^{-1} becomes weaker and shifts to 3264 cm^{-1}. It is suggested that OAHSB can also form hydrogen bond with Ch^+. As compared to TMA^+, TEA^+ and TBA^+, the Ch^+ has –OH group, which can form extra hydrogen bonds with OAHSB to motivate the self-assembly and entanglement of micelle. The hydrogen-bonding interaction between Ch^+-OAHSB is considered to be an important reason for the highest affinity of F0-D1 components. HBA structures should also cause the different binding affinity of CFF components. Given an increased electron-donating capability of $-CH_3$ < $-CH_2CH_2OH$ < $-C_2H_3$ < $-C_4H_9$ (Smith and March, 2006), the electron density of HBA cations increases in the order of $TMA^+ < Ch^+ < TEA^+ < TBA^+$. As the result, the electrostatic shielding effect of HBA cations for OAHSB molecules decreases in the order of $TMA^+ > Ch^+ > TEA^+ > TBA^+$ (see Fig. 5(d)). A stronger electrostatic shielding is favorable for the gathering and entanglement of wormlike micelles to form large micelle network structures. Furthermore, the longer the alkane groups, the larger the steric hindrance of HBA cations. For TBA^+, the large steric hindrance will reduce the intermolecular interactions of CFF components and thus restrict micelle formation, leading to the weakest affinity of F0-D4 components (Lin et al., 2020). Among those HBA cations, TMA^+ has the strongest electrostatic shielding and smallest steric hindrance. However, the Ch^+ maximizes the bonding affinity between F0 components. This is probably because the Ch^+-OAHSB hydrogen bond plays a dominant role in adjusting the bonding affinity. The addition of DES is more beneficial to improve the performance of fracturing fluids than single HBA or HBD (Figs. S13–S15 and Table S2). In addition, HBA (e.g., ChCl) enhanced the rheological properties of F0 more effectively than HBD (i.e., malonic acid). This is attributed to the electrostatic interaction between HBA cation and OAHSB. Overall, the DESs improve rheological characteristics of CFFs mainly from three steps: (1) the formation of hydrogen-bonding interactions between OAHSB and DES components; (2) the formation electrostatic interactions between HBA cations and OAHSB; and (3) the steric hindrance of HBA cations change the interaction strength of CFF components.

3.3. Performance evaluation of CFFs

For the application of CFFs, other properties (e.g., temperature resistance, salt tolerance, drag reduction, gel-breaking and spontaneous imbibition capacity) should also be concerned. Thus, those properties were explored in this section.

3.3.1. Temperature resistance

The temperature resistance of the CFFs was firstly performed at 20–90 °C under the shear rate of 170 s^{-1}. The increase in temperature results in the reduction of CFF viscosities (see Fig. 6). Similar results have been previously reported by Yang et al. (2020) and Mao et al. (2018). It suggests that high temperature can lead to the dissociation of micelles in CFFs. The viscosities of F0, F0-D1, F0-D2, F0-D3 and F0-D4 are decreased by 85.1%, 70.5%, 73.6%, 77.3% and 91.8%, respectively. Note that, F0-D1, F0-D2, F0-D3 have lower reduction rates of viscosity when compared to F0, most probably as a result of the strong interactions between D1–D3 components and OAHSB, improving the strength of micelles and thus temperature resistance of F0 system.

3.3.2. Salt resistance

The salt tolerance experiment of CFFs was carried out. The results are presented in Fig. 7. As the increase in NaCl concentration, the viscosities of CFFs are decreased (see Fig. 7(a)). Excessive NaCl could inhibit the formation of worm-like micelles because the electrostatic double layer of OAHSB surfactant was over compressed, thereby reducing the viscosity of CFF (Sun et al., 2019). D1–D3 greatly improves the NaCl resistance of F0 CFF, that is, the reduction efficiency of F0 viscosity is decreased from 71.8% to 35.8%–48.8% at the NaCl concentration of 100,000 mg·L^{-1}. Low-concentration $CaCl_2$ increases the viscosities of CFFs (see Fig. 7(b)) because Ca^{2+} ions reduce the repulsion between surfactant molecules by shielding the charges of surfactant, which is conducive to the formation micelle and thus the enhancement of micelle network strength (Al-Sadat et al., 2014). Upon $CaCl_2$ concentration to 6000 mg·L^{-1}, the viscosity of the CFFs with DESs is still increased, while that of F0 without DES is decreased, denoting that DESs enhance the salt tolerance of CFFs. This may be ascribed to the malonic acid of DESs, which interacts with Ca^{2+} by coordination-bonding interaction to weaken the compression of Ca^{2+} for the electrostatic double layer of OAHSB. According to the FT-IR analysis (Fig. S16), the C=O peak of malonic acid at 1737 cm^{-1} was shifted to at 1727 cm^{-1} when introducing Ca^{2+}. The results confirm the generation of coordination-bonding interaction between malonic acid and Ca^{2+}. DESs provides a feasibility to prepare fracturing fluids through using formation water with high salinity.

3.3.3. Drag reduction

Fig. 8 shows the drag reduction efficiency of OAHSB-based CFFs at 20–65 L·min^{-1}. The drag reduction efficiencies of F0, F0-D2 and F0-D3 are first improved and then decreased with increasing flow rate. The improvement of drag reduction efficiencies indicates that

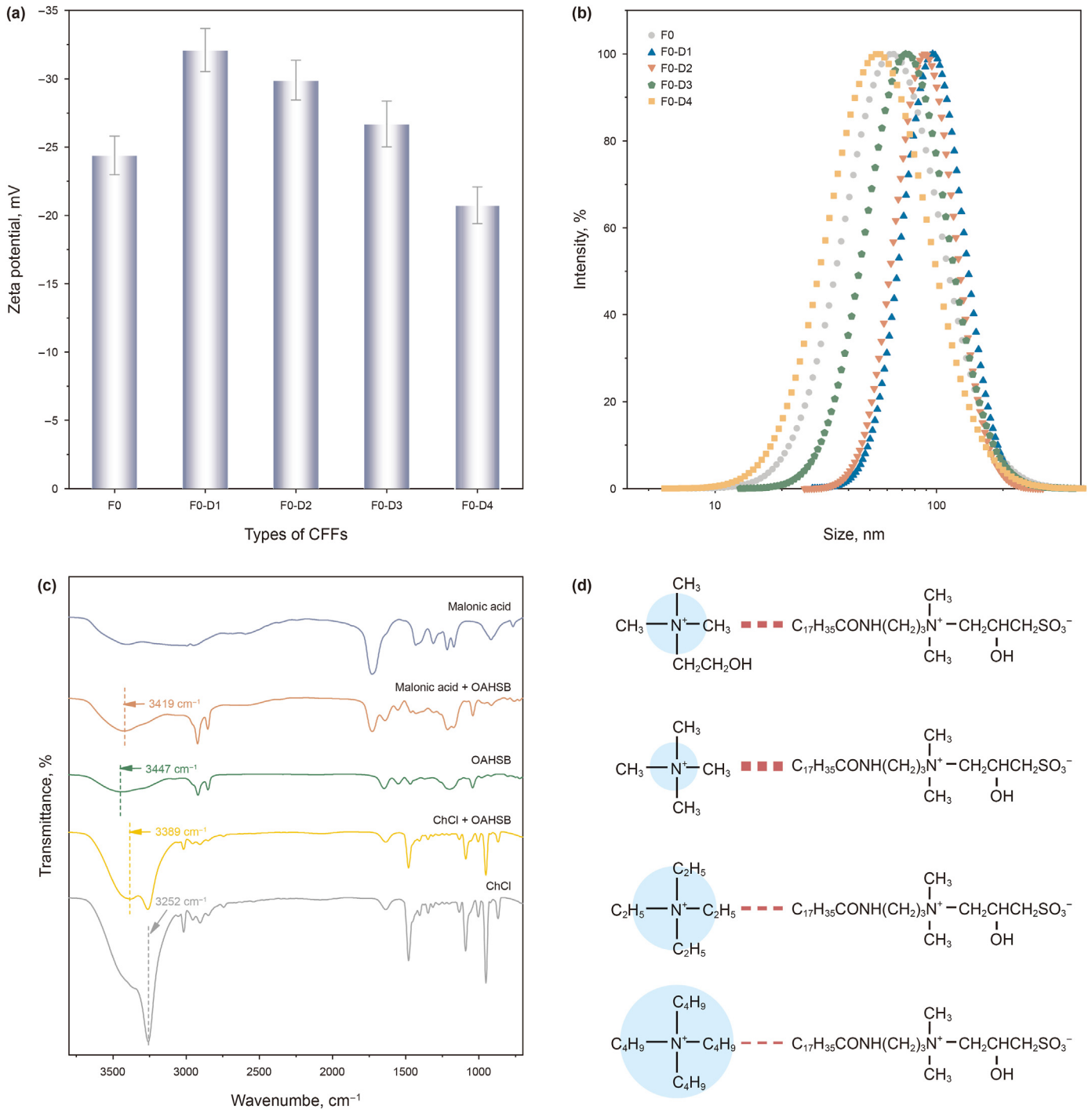

Fig. 5. Zeta potential (**a**) and micelle size (**b**) of the OAHSB-based CFFs; (**c**) FT-IR of malonic acid, ChCl, OAHSB, ChCl/OAHSB mixture and malonic acid/OAHSB mixture; (**d**) Schematic diagram for electrostatic shielding of HBA cations for OAHSB. The blue zooms are the electrons over HBA cations. The red lines indicate electrostatic shielding.

shear force stretches the micelle network in CFFs and thus suppresses the formation of turbulence (Wang et al., 2016). However, a stronger shear force can destroy the micelle network, resulting in the reduction of drag reduction efficiency. For F0-D1, the drag reduction efficiency still increases at 65 L·min^{-1}, reaching 80.3%. This means that F0-D1 has the strongest micelle network among those OAHSB-based CFFs, which is consistent with the result of steady shear test (Fig. 3b**)**. The intermolecular interactions (e.g., hydrogen-bonding interactions) brought about by the introduction of D1 components should be an important reason for the high-strength micelle network of F0-D1. By the way, for F0-D4, drag reduction efficiency exhibits a continuous decrease, implying that the weak micelle network is easily damaged by shear force.

3.3.4. *Gel breaking*

The gel-breaking performance of CFFs is evaluated, as shown in Fig. 9. All viscosities of the OAHSB-based CFFs at 170 s^{-1} are reduced after the addition of kerosene. Notably, F0-D1, F0-D2 and F0-D3 exhibit better gel-breaking performance, although their initial viscosities are higher than that of F0. The results demonstrate

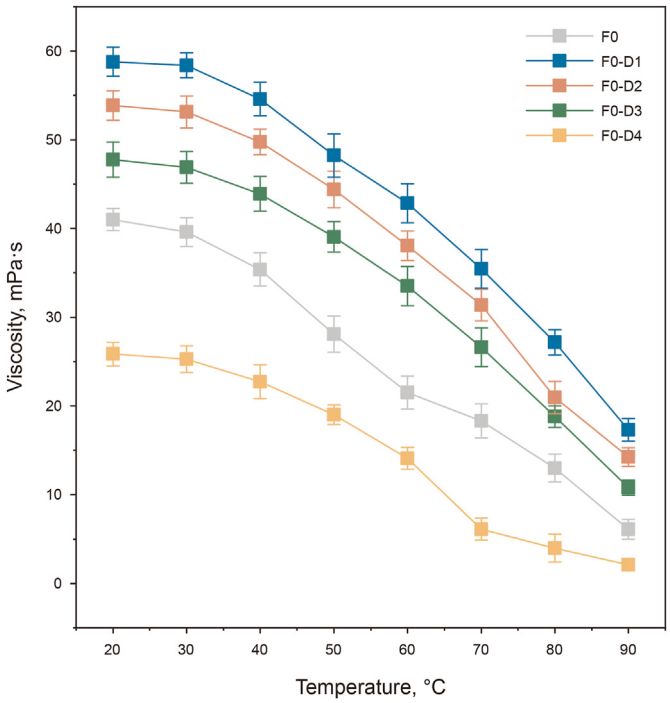

Fig. 6. Effect of temperature on the viscosity of OAHSB-based CFFs under the shear rate of 170 s^{-1}.

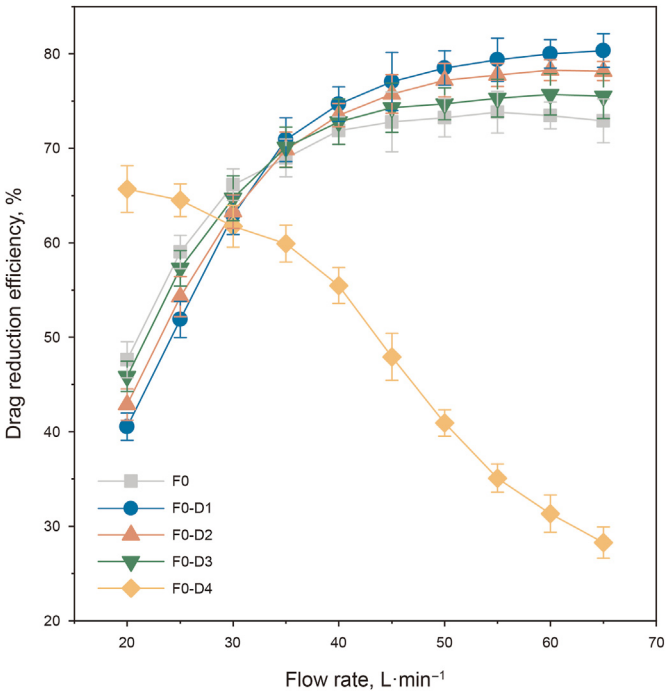

Fig. 8. Effect of flow rate on the drag reduction efficiency of CFFs.

that DESs can improve the gel-breaking performance of CFF, which is beneficial to a faster completion of gel breaking after reservoirs are fractured for subsequent construction. The reason may be that the DESs improve the strength of interactions between the components of CFF phase and oil phase, driving more oil droplets into the micelles and destroying the micelle structures (Guo et al., 2013).

3.3.5. Spontaneous imbibition

Apart from above performances, the spontaneous imbibition performance of gel-breaking CFFs is also significant. Fig. 10(a) provides the spontaneous imbibition results of gel-breaking CFF systems at 80 °C. After 98 h, the imbibition efficiency of F0 is only 29.9%. However, the considerable imbibition efficiencies of 32.1%–44.2% for F0-D1, F0-D2, F0-D3 and F0-D4 are achieved. The increased imbibition efficiencies are dependent on the introduction of DESs. Furthermore, the imbibition kinetics is also enhanced in CFF systems with D1–D4. For instance, the imbibition equilibrium of the F0-D1 system can be obtained at 74 h, which is ~24 h shorter than that of the F0 system. We hypothesize that the D1–D4

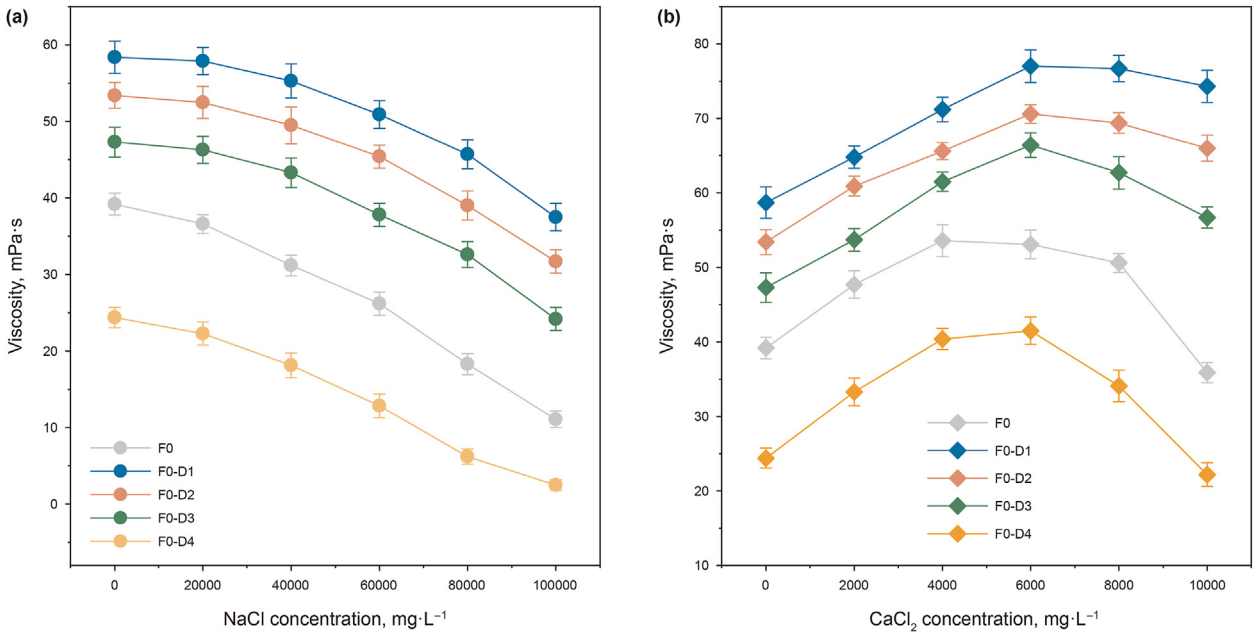

Fig. 7. Effects of NaCl (**a**) and $CaCl_2$ (**b**) concentrations on the viscosities of OAHSB-based CFFs at 170 s^{-1}.

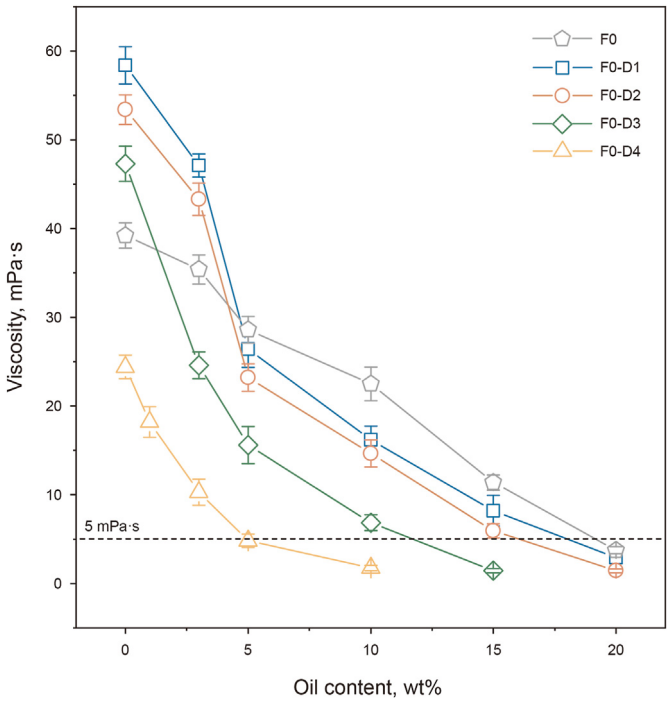

Fig. 9. Gel-breaking performance of CFFs.

effectively reduce the oil–water interface tension to promote the removal of oil from core pores, thereby accelerating the imbibition acceleration. To confirm this hypothesis, the IFT between gel-breaking CFFs and simulated oil was analyzed. According to the IFT results (see Fig. 10(b)), the D1–D3 DESs decrease the interface tension between oil and F0 phases from 0.67 to 0.30–0.44 mN·m^{-1}, which facilitates the removal of oil. However, D4 increases the interface tension to 0.71 mN·m^{-1}.

Interestingly, the imbibition efficiency of the F0-D4 system (32.1%) is higher than that of F0 (29.9%) although the interface tension of F0-D4 is the highest. Probably because the DES components can generate extra interactions with oil molecule. Table 5 describes the residual ratio of heteroatoms (i.e., S, N and O) in simulated oil after imbibition in the OAHSB-based CFF systems. After the imbibition at 80 °C for 98 h, the heteroatoms in oil are found to be obviously decreased, indicating the interactions (e.g., hydrogen bonds) between CFF system and oil droplet. According to the FT-IR, two typical peaks located at 1621 and 3416 cm^{-1} relate to the stretching vibration of C–O and O–H groups of oil (see Fig. 11(a)). And the O–H stretching vibration peaks of OAHSB and D1-D4 are observed at about 3427 cm^{-1}. Oil molecules tend to form hydrogen-bonding interactions (e.g., O–H···O, O–H···S, and O–H···N) with the CFF components, promoting the imbibition process of oil (Li et al., 2013, 2018b). Even so, the heteroatom residual ratios of imbibed oil are further reduced as the introduction of DES1-DES4 into F0. It seems that the D1–D4 enhance the strength of interactions between F0 system and oil molecule. To prove the strength enhancement of interactions, the adhesion between oil and hydrophilic glass sheet in gel-breaking CFFs was measured by AFM. The adhesion is defined as the most negative value of the force curve for probe retraction. A weak adhesion (0.12 nN) can be observed when conducted in the F0 system (see Fig. 11(b)). After replacing the liquid phase by DES-based CFF systems, the adhesion increases to 0.78–1.43 nN (see Fig. 11(c)–(f)), indicating that DESs effectively improve the oil-CFF interaction strength. In summary, these results reveal that the DESs are capable to improve the imbibition performance of CFFs from two aspects: (1) the manipulation of IFT between oil and gel-breaking CFFs; and

Table 5
The heteroatom residual ratio of simulated oil after imbibition in CFFs.

Oil	System	Residual ratio, wt%		
		S	N	O
O_0	F0	81.4	90.5	84.2
O_1	F0-D1	65.4	72.0	67.8
O_2	F0-D2	67.2	76.5	71.4
O_3	F0-D3	70.9	80.8	74.4
O_4	F0-D4	72.7	85.7	76.5

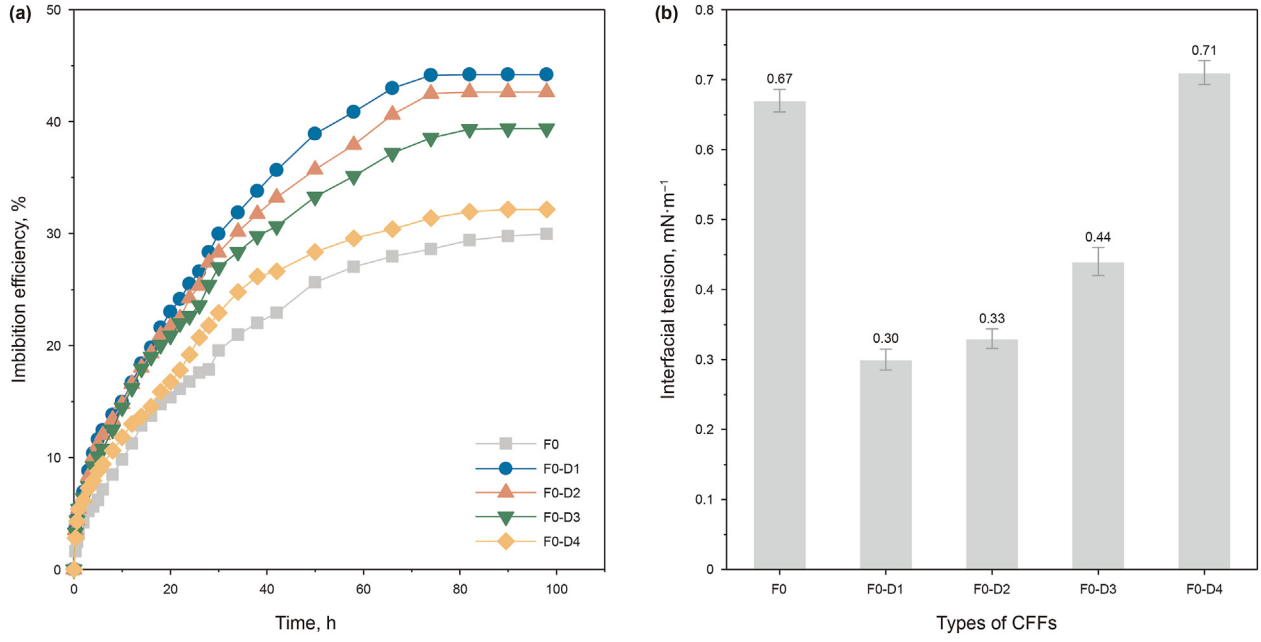

Fig. 10. Imbibition efficiency (**a**) and IFT (**b**) between gel-breaking CFFs and simulated oil.

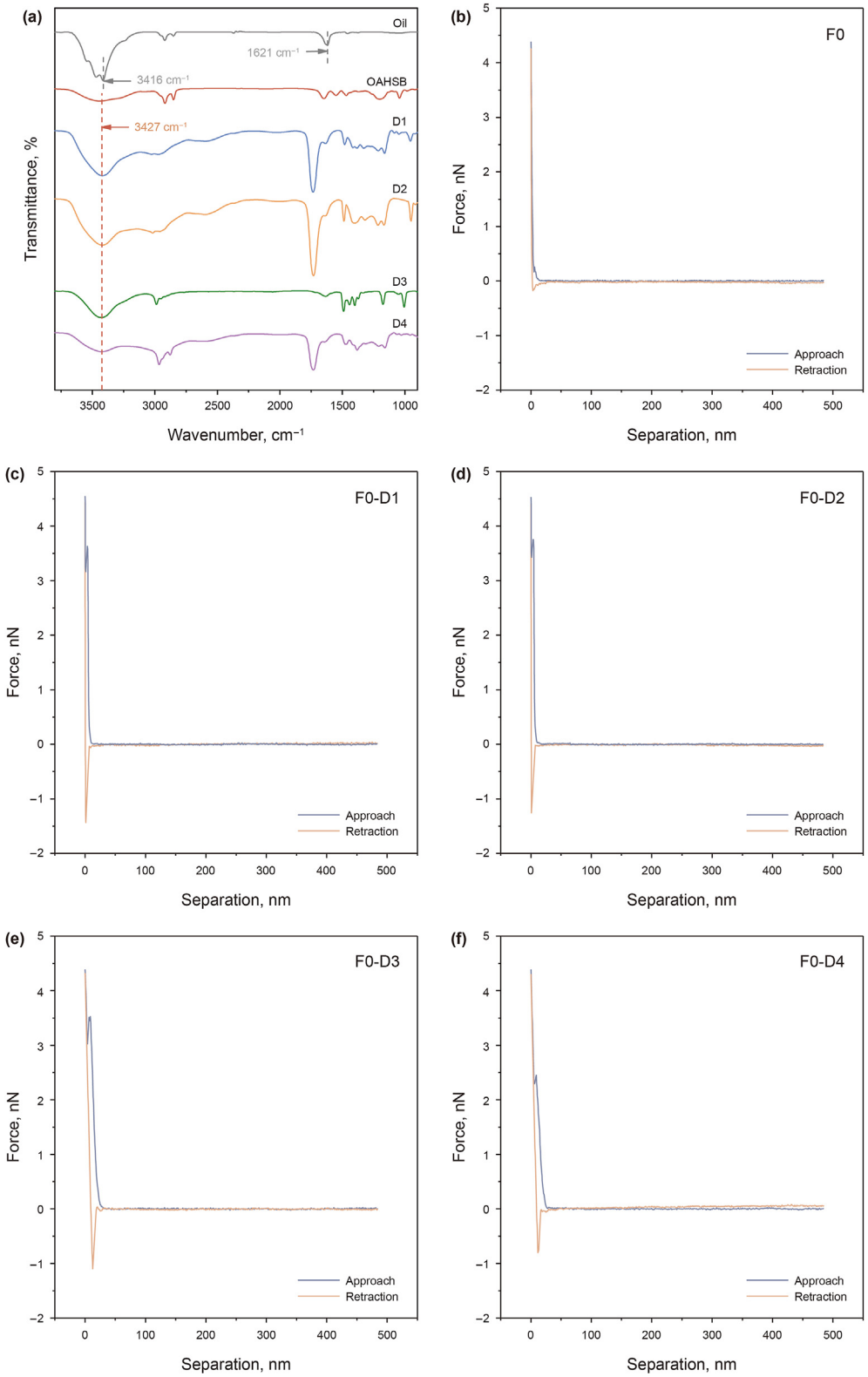

Fig. 11. (**a**) FT-IR of oil, OAHSB and D1-D4. Typical force–distance curves between the hydrophobic probe and glass sheet in F0 (**b**), F0-D1 (**c**), F0-D2 (**d**), F0-D3 (**e**) and F0-D4 (**f**).

(2) the interactions between oil and DES components.

From the above imbibition experiment results, DESs are confirmed to be useful for enhancing oil recovery. In order to compare with the imbibition results in this work, the previous reported results applying other imbibition agents such as nanofluid, ionic liquid (IL), brine, and surfactant were also investigated (see Fig. 12). It is found that brine tends to imbibe little oil even at a long imbibition time, most likely due to the absence of surface

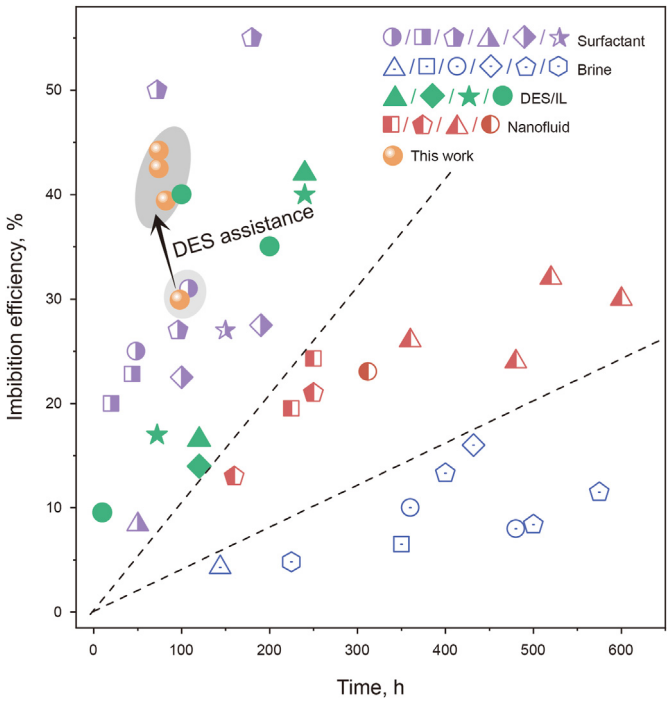

Fig. 12. Imbibition efficiency of oil in representative gel-breaking CFFs and other systems, including brine (Al-Weheibi et al., 2015; Li et al., 2018a; Manshad et al., 2017; Strand et al., 2008; Zaeri et al., 2018; Zhao et al., 2018), surfactant (Chen and Schechter, 2021; Li et al., 2022; Qi et al., 2022; Sun et al., 2021; Zhang et al., 2021a; Zhao et al., 2018), nanofluid (Li et al., 2018a; Nowrouzi et al., 2019; Zhao et al., 2020; Zhou et al., 2019a) and DES/IL (Al-Weheibi et al., 2015; Manshad et al., 2017; Sakthivel and Elsayed, 2021; Shuwa et al., 2015).

activity. The nanofluid is more conductive to achieve relatively high imbibition efficiencies, since nanoparticles are capable of decreasing oil–water IFT and altering the wettability of rock surface, but taking longer to achieve higher imbibition efficiency. Remarkably, the surfactant, DES and IL solutions can achieve high imbibition efficiencies during short imbibition period.

When employing DESs to assist the surfactant solution to imbibe oil from cores, a better imbibition performance can be obtained. For example, the imbibition efficiency of the F0 system is only 29.9% at 98 h, which apparently promote to ~39.4%–44.2% within 90 h by introducing D1–D3 DESs. However, some oil is still hard to be removed from the pores of cores, which should be attributed to the low permeability and heterogeneity of the cores (Kong et al., 2021). Anyhow, the DESs in this work have confirmed the feasibility for effectively promoting the imbibition performance of CFFs.

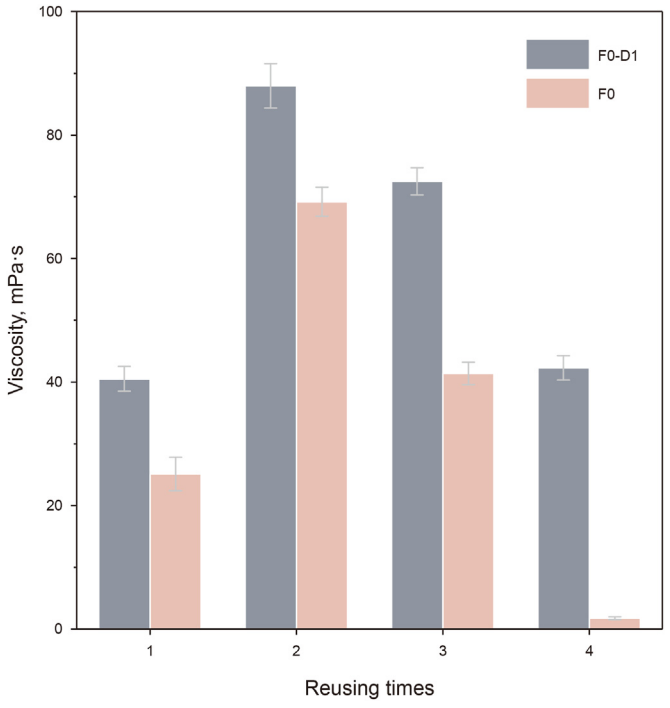

Fig. 13. Viscosity of solutions prepared by reused gel-breaking F0-D1 and F0.

3.4. Reusing of gel-breaking CFFs

From economic and environmental aspects, the reusing of gel-breaking CFFs after flowback is critical. The gel-breaking F0 and F0-D1 were selected as examples to explore the feasibility of reusing gel-breaking CFFs (see Supporting information 1.1), using the viscosity of solution prepared with gel-breaking CFF and 0.5 wt % OAHSB as an evaluation criterion. With the increase in recycling times, the viscosities of prepared solutions remarkably increase and then decrease (see Fig. 13). The F0-D1-based solutions exhibit higher viscosities than the F0-based solutions. After four cycles, the viscosity of F0-D1-based solution can reach 42.3 mPa·s, while that of F0-based solution is only 1.7 mPa·s. Good reusing stability of the gel-breaking F0-D1 reveals DESs provide excellent potential to prepare CFF utilizing gel-breaking CFF.

4. Conclusions

Four binary DESs were prepared as the “green” additives to explore their underlying effect on the properties of CFFs on the basis of intermolecular interactions. The DES components enhanced the CFF properties through their hydrogen-bonding and electrostatic interactions with OAHSB molecules. Among those DESs, the D1 reduced the CMC of OAHSB from 32 to 17 μM and the γ_{CMC} from 35.1 to 33.8 $mN \cdot m^{-1}$. Moreover, the D1 excellently promoted the formation and entanglement of micelles in CFF to improve micelle network strength and thus the CFF properties (e.g., rheology, temperature resistance, salt tolerance, drag reduction, and gel breaking). The coordination-bonding interaction between OAHSB and malonic acid HBD plays an important role in improving the Ca^{2+} resistance of CFF. For spontaneous imbibition test, the imbibition efficiency was increased from 29.9% in 98 h to 44.2% in 74 h because the introduction of DESs strengthens the CFF solution–oil interactions. The adjustment of HBAs is capable of improving the CFF properties by regulating the intermolecular interactions (e.g., HBA-OAHSB and OAHSB-OAHSB interactions). These results provide a new perspective for employing DESs to effectively improve CFF property.

Declaration of competing interest

The authors declare that they have no known competing financial interests or personal relationships that could have appeared to influence the work reported in this paper.

Acknowledgment

The authors appreciate the support from the National Natural Science Foundation of China (Nos. 52120105007, 51834010), and the National Science Fund for Distinguished Young Scholars (No. 52222403).

Appendix A. Supplementary data

Supplementary data to this article can be found online at https://doi.org/10.1016/j.petsci.2023.08.013.

References

Acharya, D.P., Sato, T., Kaneko, M., Singh, Y., Kunieda, H., 2006. Effect of added poly(oxyethylene)dodecyl ether on the phase and rheological behavior of wormlike micelles in aqueous SDS solutions. J. Phys. Chem. B 110, 754–760. https://doi.org/10.1021/jp054631x.

Al-Sadat, W., Nasser, M.S., Chang, F., Nasr-El-Din, H.A., Hussein, I.A., 2014. Rheology of a viscoelastic zwitterionic surfactant used in acid stimulation: effects of surfactant and electrolyte concentration. J. Petrol. Sci. Eng. 124, 341–349. https://doi.org/10.1016/j.petrol.2014.09.014.

Al-Weheibi, I., Al-Hajri, R., Al-Wahaibi, Y., Jibril, B., Mohsenzadeh, A., 2015. Oil recovery enhancement in middle east heavy oil field using malonic acid based deep eutectic solvent. In: SPE Middle East Oil & Gas Show and Conference. https://doi.org/10.2118/172592-MS.

Atilhan, M., Aparicio, S., 2022. Molecular dynamics study on the use of deep eutectic solvents for enhanced oil recovery. J. Petrol. Sci. Eng. 209, 109953. https://doi.org/10.1016/j.petrol.2021.109953.

Chen, W.D., Schechter, D.S., 2021. Surfactant selection for enhanced oil recovery based on surfactant molecular structure in unconventional liquid reservoirs. J. Petrol. Sci. Eng. 196, 107702. https://doi.org/10.1016/j.petrol.2020.107702.

Cheng, R., Meng, F.H., Deng, C., Klok, H.A., Zhong, Z.Y., 2013. Dual and multi-stimuli responsive polymeric nanoparticles for programmed site-specific drug delivery. Biomaterials 34 (14), 3647–3657. https://doi.org/10.1016/j.biomaterials.2013.01.084.

Chu, Z.L., Dreiss, C.A., Feng, Y.J., 2013. Smart wormlike micelles. Chem. Soc. Rev. 42 (17), 7174–7203. https://doi.org/10.1039/C3CS35490C.

de Aguiar, H.B., de Beer, A.G.F., Strader, M.L., Roke, S., 2010. The interfacial tension of nanoscopic oil droplets in water is hardly affected by SDS surfactant. J. Am. Chem. Soc. 132 (7), 2122–2123. https://doi.org/10.1021/ja9095158.

Feng, D., Zhang, Y.M., Chen, Q.S., Wang, J.Y., Li, B., Feng, Y.J., 2012. Synthesis and surface activities of amidobetaine surfactants with ultra-long unsaturated hydrophobic chains. J. Surfactants Deterg. 15 (5), 657–661. https://doi.org/10.1007/s11743-012-1359-7.

Guo, W.J., Hou, Y.C., Wu, W.Z., Ren, S.H., Tian, S.D., Marsh, K.N., 2013. Separation of phenol from model oils with quaternary ammonium salts via forming deep eutectic solvents. Green Chem. 15, 226–229. https://doi.org/10.1039/C2GC36602A.

Hadj-Kali, M.K., Al-khidir, K.E., Wazeer, I., El-blidi, L., Mulyono, S., AlNashef, I.M., 2015. Application of deep eutectic solvents and their individual constituents as surfactants for enhanced oil recovery. Colloids Surf. A Physicochem. Eng. Asp. 487, 221–231. https://doi.org/10.1016/j.colsurfa.2015.10.005.

Hao, X., Leng, Z.J., Wang, H.R., Peng, F., Yan, Q., 2020. CO_2-switchable non-Newtonian fluids. Green Chem. 22, 3784–3790. https://doi.org/10.1039/d0gc00877j.

Javadi, A.H., Fatemi, M., 2022. Impact of salinity on fluid/fluid and rock/fluid interactions in enhanced oil recovery by hybrid low salinity water and surfactant flooding from fractured porous media. Fuel 329, 125426. https://doi.org/10.1016/j.fuel.2022.125426.

Jin, D.Y., Yu, G.J., Li, X.Y., Li, T.H., Zhang, F., Tian, S.C., Zhou, Z.Y., Ren, Z.Q., 2022. One-pot extractive and oxidative desulfurization of fuel with ternary dual-acid deep eutectic solvent. Fuel 329, 125513. https://doi.org/10.1016/j.fuel.2022.125513.

Kawai, S., Foster, A.S., Bjorkman, T., Nowakowska, S., Bjork, J., Canova, F.F., Gade, L.H., Jung, T.A., Meyer, E., 2016. Van der Waals interactions and the limits of isolated atom models at interfaces. Nat. Commun. 7 (1), 11559. https://doi.org/10.1038/ncomms11559.

Kelleppan, V.T., King, J.P., Butler, C.S.G., Williams, A.P., Tuck, K.L., Tabor, R.F., 2021. Heads or tails? The synthesis, self-assembly, properties and uses of betaine and betaine-like surfactants. Advan. Colloid and Interf. Sci. 297, 102528. https://doi.org/10.1016/j.cis.2021.102528.

Kong, S.Q., Feng, G., Liu, Y.L., Li, K.J., 2021. Potential of dimethyl ether as an additive in CO_2 for shale oil recovery. Fuel 296, 120643. https://doi.org/10.1016/j.fuel.2021.120643.

Kuang, W.D., Saraji, S., Piri, M., 2018. A systematic experimental investigation on the synergistic effects of aqueous nanofluids on interfacial properties and their implications for enhanced oil recovery. Fuel 220, 849–870. https://doi.org/10.1016/j.fuel.2018.01.102.

Lee, T., Bocquet, L., Coasne, B., 2016. Activated desorption at heterogeneous interfaces and long-time kinetics of hydrocarbon recovery from nanoporous media. Nat. Commun. 7, 11890. https://doi.org/10.1038/ncomms1189.

Li, C.P., Li, D., Zou, S.S., Li, Z., Yin, J.M., Wang, A.L., Cui, Y.N., Yao, Z.L., Zhao, Q., 2013. Extraction desulfurization process of fuels with ammonium-based deep eutectic solvents. Green Chem. 15, 2793–2799. https://doi.org/10.1039/C3GC41067F.

Li, L., Sun, Y., Li, Y., Wang, R.Y., Chen, J., Wu, Y.N., Dai, C.L., 2022. Interface properties evolution and imbibition mechanism of gel breaking fluid of clean fracturing fluid. J. Mol. Liq. 359, 118952. https://doi.org/10.1016/j.molliq.2022.118952.

Li, Y.Y., Dai, C.L., Zhou, H.D., Wang, X.K., Lv, W.J., Zhao, M.W., 2018a. Investigation of spontaneous imbibition by using a surfactant-free active silica water-based nanofluid for enhanced oil recovery. Energy Fuel. 32, 287–293. https://doi.org/10.1021/acs.energyfuels.7b03132.

Li, Z.H., Liu, D., Men, Z.W., Song, L.H., Lv, Y.J., Wu, P.P., Lou, B., Zhang, Y.D., Shi, N., Chen, Q.T., 2018b. Insight into effective denitrification and desulfurization of liquid fuel with deep eutectic solvents: an innovative evaluation criterion to filtrate extractants using the compatibility index. Green Chem. 20 (13), 3112–3120. https://doi.org/10.1039/C8GC00828K.

Lin, S.Q., Xu, C., Xu, L., Wang, Z.L., 2020. The overlapped electron-cloud model for electron transfer in contact electrification. Adv. Funct. Mater. 30 (11), 1909724. https://doi.org/10.1002/adfm.201909724.

Liu, J.R., Shen, J.J., Wang, X.K., Ge, H.K., Yao, E.D., 2019. Experimental study of wettability alteration and spontaneous imbibition in Chinese shale oil reservoirs using anionic and nonionic surfactants. J. Petrol. Sci. Eng. 175, 624–633. https://doi.org/10.1016/j.petrol.2019.01.003.

Liu, Z.L., Bode, V., Hadayati, P., Onay, H., Sudholter, E.J.R., 2020. Understanding the stability mechanism of silica nanoparticles: the effect of cations and EOR chemicals. Fuel 280, 118650. https://doi.org/10.1016/j.fuel.2020.118650.

Ma, L., Li, G.Q., Xu, H.M., Liu, Z.Y., Wan, Q., Liu, D.Y., Shen, Q.R., 2022. Structural and functional study of a novel lytic polysaccharide monooxygenase $cPMO_2$ from compost sample in the oxidative degradation of cellulose. Chem. Eng. J. 433, 134509. https://doi.org/10.1016/j.cej.2022.134509.

Manshad, A.K., Rezaei, M., Moradi, S., Nowrouzi, I., Mohammadi, A.H., 2017. Wettability alteration and interfacial tension (IFT) reduction in enhanced oil recovery (EOR) process by ionic liquid flooding. J. Mol. Liq. 248, 153–162. https://doi.org/10.1016/j.molliq.2017.10.009.

Mao, J.C., Yang, X.J., Chen, Y.A., Zhang, Z.Y., Zhang, C., Yang, B., Zhao, J.Z., 2018. Viscosity reduction mechanism in high temperature of a Gemini viscoelastic surfactant (VES) fracturing fluid and effect of counter-ion salt (KCl) on its heat resistance. J. Petrol. Sci. Eng. 164, 189–195. https://doi.org/10.1016/j.petrol.2018.01.052.

Nowrouzi, I., Manshad, A.K., Mohammadi, A.H., 2019. Effects of concentration and size of TiO_2 nano-particles on the performance of smart water in wettability alteration and oil production under spontaneous imbibition. J. Petrol. Sci. Eng. 183, 106357. https://doi.org/10.1016/j.petrol.2019.106357.

Qi, Z., Han, M., Chen, S., Wang, J., 2022. Surfactant enhanced imbibition in carbonate reservoirs: effect of IFT reduction and surfactant partitioning. JCIS Open 5, 100045. https://doi.org/10.1016/j.jciso.2022.100045.

Raj, K.A., Balikram, A., Ojha, K., 2022. Impact assessment of nanoparticles on microstructure and rheological behaviour of VES fracturing fluid formulated with mixed surfactant system. J. Mol. Liq. 345, 118241. https://doi.org/10.1016/j.molliq.2021.118241.

Rosen, M.J., 2004. Surfactants and Interfacial Phenomena. John Wiley & Sons, Inc.

Sakthivel, S., Elsayed, M., 2021. Enhanced oil recovery by spontaneous imbibition of imidazolium based ionic liquids on the carbonate reservoir. J. Mol. Liq. 340, 117301. https://doi.org/10.1016/j.molliq.2021.117301.

Sakthivel, S., Velusamy, S., Nair, V.C., Sharma, T., Sangwai, J.S., 2016. Interfacial tension of crude oil-water system with imidazolium and lactam-based ionic liquids and their evaluation for enhanced oil recovery under high saline environment. Fuel 191, 239–250. https://doi.org/10.1016/j.fuel.2016.11.064.

Sanati, A., Rahmani, S., Nikoo, A.H., Malayeri, M.R., Busse, O., Weigand, J.J., 2021. Comparative study of an acidic deep eutectic solvent and an ionic liquid as chemical agents for enhanced oil recovery. J. Mol. Liq. 329, 115527. https://doi.org/10.1016/j.molliq.2021.115527.

Scholz, C., Ldov, A., Poschel, T., Engel, M., Lowen, H., 2021. Surfactants and rotelles in active chiral fluids. Sci. Adv. 7 (16), eabf8998. https://doi.org/10.1126/sciadv.abf8998.

Shuwa, S.M., Jibril, B.Y., Al-Wahaibi, Y.M., Al-Hajri, R.S., 2015. Heavy-oil-recovery enhancement with choline chloride/ethylene glycol-based deep eutectic solvent. SPE J. 20 (1), 79–87. https://doi.org/10.2118/172499-PA.

Smith, E.L., Abbott, A.P., Ryder, K.S., 2014. Deep eutectic solvents (DESs) and their applications. Chem. Rev. 114 (21), 11060–11082. https://doi.org/10.1021/cr300162p.

Smith, M.B., March, J., 2006. March's Advanced Organic Chemistry: Reactions, Mechanisms, and Structure. John Wiley & Sons, Inc, New York.

Strand, S., Puntervold, T., Austad, T., 2008. Effect of temperature on enhanced oil recovery from mixed-wet chalk cores by spontaneous imbibition and forced displacement using seawater. Energy Fuel. 22, 3222–3225. https://doi.org/10.1021/ef800244v.

Su, H.C., Fang, F.C., Hwu, T.Y., Hsieh, H.H., Chen, H.F., Lee, G.H., Peng, S.M., Wong, K.T., Wu, C.C., 2007. Highly efficient orange and green solid-state light-emitting electrochemical cells based on cationic IrIII complexes with enhanced steric hindrance. Adv. Funct. Mater. 7, 1019–1027. https://doi.org/10.1002/adfm.200600372.

Sun, X., Gao, Z.B., Zhao, M.W., Gao, M.W., Du, M.Y., Dai, C.L., 2019. Development and evaluation of a novel seawater-based viscoelastic fracturing fluid system. J. Petrol. Sci. Eng. 183, 106408. https://doi.org/10.1016/j.petrol.2019.106408.

Sun, Y.P., Xin, Y., Lyu, F.T., Dai, C.L., 2021. Experimental study on the mechanism of adsorption-improved imbibition in oil-wet tight sandstone by a nonionic surfactant for enhanced oil recovery. Petrol. Sci. 18 (4), 1115–1126. https://doi.org/10.1016/j.petsci.2021.07.005.

Tran, M.K., Rodrigues, M.T.F., Kato, K., Babu, G., Ajayan, P.M., 2019. Deep eutectic solvents for cathode recycling of Li-ion batteries. Nat. Energy 4, 339–345. https://doi.org/10.1038/s41560-019-0368-4.

Wang, H.M., Li, M.R., Garg, S., Wu, Y.M., Idros, M.N., Hocking, R., Duan, H.R., Gao, S., Yago, A.J., Zhuang, L.Z., Rufford, T.E., 2021. Cobalt Electrochemical recovery from

lithium cobalt oxides in deep eutectic choline chloride plus urea solvents. ChemSusChem 14 (14), 2972–2983. https://doi.org/10.1002/cssc.202100954.
Wang, L., Wang, D., Shen, Y.D., Lai, X.J., Guo, X., 2016. Study on properties of hydrophobic associating polymer as drag reduction agent for fracturing fluid. J. Polym. Res. 23 (11), 1–8. https://doi.org/10.1007/s10965-016-1129-8.
Wang, P., Huang, S.J., Zhao, F.L., Shi, J., Wang, B., Li, Y., 2022. Modeling phase behavior of nano-confined fluids in shale reservoirs with a modified Soave-Redlich-Kwong equation of state. Chem. Eng. J. 443, 133661. https://doi.org/10.1016/j.cej.2021.133661.
Wu, A.L., Gao, Y.A., Zheng, L.Q., 2019. Zwitterionic amphiphiles: their aggregation behavior and applications. Green Chem. 21, 4290–4312. https://doi.org/10.1039/C9GC01808E.
Wu, Y.N., Tang, L.S., Li, Y., Zhang, L.Y., Jin, X., Zhao, M.W., Feng, X., Dai, C.L., 2023. Probing the influence of secondary fracture connectivity on fracturing fluid flowback efficiency. Petrol. Sci. 20 (2), 973–981. https://doi.org/10.1016/j.petsci.2022.10.014.
Xie, Y.J., Dong, H.F., Zhang, S.J., Lu, X.H., Ji, X.Y., 2016. Solubilities of CO_2, CH_4, H_2, CO and N_2 in choline chloride/urea. Green Energy Environ. 1, 195–200. https://doi.org/10.1016/j.gee.2016.09.001.
Yang, B., Wang, H.Z., Li, G.S., Wang, B., Chang, L., Tian, G.H., Zhao, M.W., Zheng, Y., 2022. Fundamental study and utilization on supercritical CO_2 fracturing developing unconventional resources: current status, challenge and future perspectives. Petrol. Sci. 19 (6), 2757–2780. https://doi.org/10.1016/j.petsci.2022.08.029.
Yang, X.J., Mao, J.H., Mao, J.C., Jiang, Q.H., Fu, M.T., Lin, C., Chen, A., Cun, M., Du, A.Q., Xiao, S.Y., Zhao, J.Z., 2020. The role of KCl in cationic Gemini viscoelastic surfactant based clean fracturing fluids. Colloids Surf. A Physicochem. Eng. Asp. 606, 125510. https://doi.org/10.1016/j.colsurfa.2020.125510.
Yin, H.Y., Yin, X., Cao, R.B., Zeng, P.Y., Wang, J., Wu, D.G., Luo, X.J., Zhu, Y.Y., Zheng, Z., Feng, Y.J., 2022. In situ crosslinked weak gels with ultralong and tunable gelation times for improving oil recovery. Chem. Eng. J. 432, 134350. https://doi.org/10.1016/j.cej.2021.134350.
Zaeri, M.R., Hashemi, R., Shahverdi, H., Sadeghi, M., 2018. Enhanced oil recovery from carbonate reservoirs by spontaneous imbibition of low salinity water. Petrol. Sci. 15 (3), 564–576. https://doi.org/10.1007/s12182-018-0234-1.
Zhang, K.Q., Jin, Z.J., Li, S.Y., 2022a. Coupled miscible carbon utilization-storage processes in fractured shales. Chem. Eng. J. 441, 135987. https://doi.org/10.1016/j.cej.2022.135987.
Zhang, L.Y., Abbaspourrad, A., Parsa, S., Tang, J.Z., Cassiola, F., Zhang, M., Tian, S.C., Dai, C.L., Xiao, L.Z., Weitz, D.A., 2020. Core-shell nanohydrogels with programmable swelling for conformance control in porous media. ACS Appl. Mater. Interfaces 12 (30), 34217–34225. https://doi.org/10.1021/acsami.0c09958.
Zhang, Q.H., Vigier, K.D., Royer, S., Jerome, F., 2012. Deep eutectic solvents: syntheses, properties and applications. Chem. Soc. Rev. 41 (21), 7108–7146. https://doi.org/10.1039/C2CS35178A.
Zhang, X., Liu, D.X., Liu, Y., Li, L.L., Yuan, J., 2021a. Synergistic effects between anionic and amphoteric surfactants on promoting spontaneous imbibition in ultra-low permeability reservoirs: study of mechanism and formula construction. Colloids Surf. A Physicochem. Eng. Asp. 625, 126930. https://doi.org/10.1016/j.colsurfa.2021.126930.
Zhang, Y., Mao, J.C., Zhao, J.Z., Liao, Z.J., Xu, T., Mao, J.H., Sun, H.L., Zheng, L.J., Ni, Y.H., 2021b. Synergy between different sulfobetaine-type zwitterionic Gemini surfactants: surface tension and rheological properties. J. Mol. Liq. 332, 115141. https://doi.org/10.1016/j.molliq.2020.115141.
Zhang, Y., Mao, J.C., Zhao, J.Z., Yang, X.J., Zhang, Z.Y., Yang, B., Zhang, W.L., Zhang, H., 2018. Preparation of a novel ultra-high temperature low-damage fracturing fluid system using dynamic crosslinking strategy. Chem. Eng. J. 354, 913–921. https://doi.org/10.1016/j.cej.2018.08.021.
Zhang, Y.M., Mu, M., Yang, Z., Liu, X.C., 2022b. Ultralong-chain ionic liquid surfactants derived from natural erucic acid. ACS Sustain. Chem. Eng. 10 (7), 2545–2555. https://doi.org/10.1021/acssuschemeng.1c08558.
Zhao, G., Yan, Z.H., Qian, F., Sun, H.N., Lu, X., Fan, H.M., 2019. Molecular simulation study on the rheological properties of a pH-responsive clean fracturing fluid system. Fuel 253, 677–684. https://doi.org/10.1016/j.fuel.2019.05.027.
Zhao, M.W., Lv, W.J., Li, Y.Y., Dai, C.L., Wang, X.K., Zhou, H.D., Zou, C.W., Gao, M.W., Zhang, Y., Wu, Y.N., 2018. Study on the synergy between silica nanoparticles and surfactants for enhanced oil recovery during spontaneous imbibition. J. Mol. Liq. 261, 373–378. https://doi.org/10.1016/j.molliq.2018.04.034.
Zhao, M.W., Song, X.G., Lv, W.J., Wu, Y.N., Dai, C.L., 2020. The preparation and spontaneous imbibition of carbon-based nanofluid for enhanced oil recovery in tight reservoirs. J. Mol. Liq. 313, 113564. https://doi.org/10.1016/j.molliq.2020.113564.
Zhou, F.J., Su, H., Liang, X.Y., Meng, L.F., Yuan, L.S., Li, X.H., Liang, T.B., 2019a. Integrated hydraulic fracturing techniques to enhance oil recovery from tight rocks. Petrol. Explor. Dev. 46 (5), 1065–1072. https://doi.org/10.1016/S1876-3804(19)60263-6.
Zhou, L., Lu, X.M., Ju, Z.Y., Liu, B., Yao, H.Y., Xu, J.L., Zhou, Q., Hu, Y.F., Zhang, S.J., 2019b. Alcoholysis of polyethylene terephthalate to produce dioctyl terephthalate using choline chloride-based deep eutectic solvents as efficient catalysts. Green Chem. 21 (4), 897–906. https://doi.org/10.1039/C8GC03791D.
Zhou, Y.X., Wu, X., Zhong, X., Sun, W., Pu, H., Zhao, J.X., 2019c. Surfactant-Augmented functional silica nanoparticle based nanofluid for enhanced oil recovery at high temperature and salinity. ACS Appl. Mater. Interfaces 11 (49), 45763–45775. https://doi.org/10.1021/acsami.9b16960.